Microwave spectroscopy of Majorana vortex modes

Zhibo Ren,[1] Justin Copenhaver [1,2] Leonid Rokhinson,[1] and Jukka I. Väyrynen [1]

[1]*Department of Physics and Astronomy, Purdue University, West Lafayette, Indiana 47907, USA*
[2]*Department of Physics, University of Colorado, Boulder, Colorado 80309, USA*

The observation of zero-bias conductance peaks in vortex cores of certain Fe-based superconductors has sparked renewed interest in vortex-bound Majorana states. These materials are believed to be intrinsically topological in their bulk phase, thus avoiding potentially problematic interface physics encountered in superconductor-semiconductor heterostructures. However, progress towards demonstration of non-Abelian statistics of vortex Majorana modes is hindered by our inability to measure the topological quantum state of a nonlocal vortex Majorana state, i.e., the charge of a vortex pair. In this paper, we theoretically propose a microwave-based charge parity readout of the Majorana vortex pair charge. A microwave resonator above the vortices can couple to the charge allowing for a dispersive readout of the Majorana parity. Our technique may also be used in vortices in conventional superconductors and allows one to probe the lifetime of vortex-bound quasiparticles, which is currently beyond existing scanning tunneling microscopy capabilities.

Introduction. Majorana zero modes were originally proposed within the context of vortices in a topological superconductor (SC) [1–5] and have since emerged as a captivating subject of study in the field of superconductivity. The recent discovery of zero-bias conductance peaks [6–14] in the vortex cores of certain Fe-based superconductors [15–19] has sparked renewed interest in vortex Majorana zero modes (MZMs), which are predicted to be bound in these vortices [5,20–23]. The inherent topological nature of vortices as excitations within the superconducting condensate gives hope that the bound states hosted by them would be less susceptible to disorder, unlike Majorana approaches that require engineered interfaces [24,25]. The key motivation behind studying MZMs is their predicted non-Abelian braiding statistics and possible use in a topologically protected quantum computer [3,26–29].

However, the measurement of the topological quantum state of a nonlocal vortex MZM remains a challenge, hindering progress toward unambiguous demonstration of non-Abelian statistics and eventual vortex-based topological qubits. While it is, in principle, possible to move the vortices and associated MZMs [30–33], it will be challenging to do this adiabatically for a large vortex, and at the same time fast enough to avoid quasiparticle poisoning, the timescale of which in vortices is currently unknown. Alternatively, measurement-based braiding techniques could potentially circumvent the need for moving the MZMs [34]. Nonlocal conductance [35,36] and interferometric [37,38] measurements have been suggested as a means to identify and control Majorana vortex modes. Nevertheless, it is important to note that a microwave-based technique would be optimal for achieving fast readout [39,40].

In this paper, we propose a solution to the measurement problem using microwave (MW) techniques, which have been established and demonstrated to be an extremely versatile tool to address electronic systems in various experiments [41–48]. Specifically, we present a microwave-based method for MZM charge parity readout analogous to what has been proposed for different platforms [39,49,50–53].

Our approach focuses on studying the coupling between electrons in an Fe-based superconductor and the microwave photons from a resonator positioned above it. By analyzing the frequency-dependent transmission of the resonator, we can achieve a dispersive readout of the nonlocal vortex Majorana state. We provide the necessary requirements for the resonator quality factor Q to enable the parity readout. Importantly, our technique can also be applied to vortices in conventional superconductors, offering insights into the lifetime and coherent manipulation of vortex-bound quasiparticles, surpassing the capabilities of the existing scanning tunneling microscopy.

General theory of MW coupling to a vortex state. The interaction between the external electromagnetic field and the charge density of the superconductor results in a MW coupling Hamiltonian:

$$\delta H \cos \omega t = \int d^3\mathbf{r} \, \rho_e(\mathbf{r}) V(\mathbf{r}) \cos \omega t, \tag{1}$$

where $\rho_e(\mathbf{r})$ is the charge density operator and $V(\mathbf{r}) \cos \omega t$ is the scalar potential of the external electromagnetic field. This electromagnetic field is created by a resonator which is within less than a wavelength of the SC surface. Thus, the MW field can be treated in the quasistatic approximation. A sketch of the measurement setup is shown in Fig. 1(a).

In the static field approximation, screening in the superconductor results in decay of the field, characterized by the screening length λ_{TF}. The scalar potential of the external electromagnetic field can be written as $V(\mathbf{r}) = V_0 e^{-\frac{z}{\lambda_{\text{TF}}}}$, where z is the distance from the top surface of the superconductor and V_0 is the amplitude of the external potential.

In Eq. (1), the charge density ρ_e can be expressed as $\rho_e = -\frac{1}{2} e \Psi^\dagger \tau_z \Psi$, where $\Psi = ((c_\uparrow, c_\downarrow), (c_\uparrow^\dagger, c_\downarrow^\dagger))^T$ is the Nambu field operator and $\tau_z = \text{diag}(1, 1, -1, -1)$. In order to expand the field operator in the exact eigenbasis of the
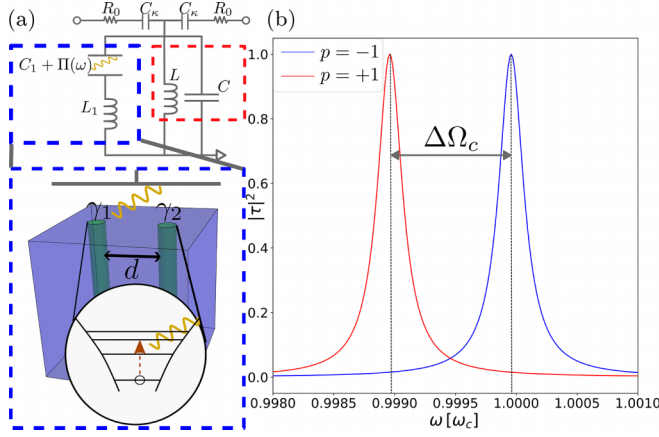
FIG. 1. Dispersive readout of vortex MZM parity. (a) Schematic circuit model. The red square shows the cavity resonator, and the blue squares show the capacitive coupling to the SC vortex state. The microwave response of the vortex pair, represented by the charge-charge correlation function $\Pi(\omega)$, depends on the MZM parity as described in Eq. (6). (b) Transmission vs frequency in the detuning regime $|E_1 - \omega_c| \gg \omega_c \zeta$, E_M. Here E_1 and E_M are the energies of the first bound state and Majorana state, ζ is the dimensionless charge [see above Eq. (8)], and ω_c is the resonant frequency of the cavity. The parity readout measures $\langle i\gamma_1\gamma_2\rangle$, the occupation number parity of the Majorana state on the top surface. We take here the first bound state energy $E_1 \approx 2\omega_c$, $E_M = 0$, $\zeta = 0.015$, and $\delta\zeta = 0.02$. These parameters correspond to the critical cavity Q factor $Q_c \approx 10^3$, and in the plot, we take $Q = 10^4 \gg Q_c$, so these peaks can clearly be resolved.

unperturbed Hamiltonian H_0 [given by Eq. (10)], we define Φ_n as the spinor wave function of the eigenstate with energy E_n and Γ_n as the second quantized annihilation operators of these quasiparticles.

The eigenstates of the system exhibit a particle-hole symmetry (PHS) that is represented by an antiunitary operator $\mathcal{P}$. For each eigenstate Φ_n with energy E_n, also another eigenstate $\Phi_{-n} = \mathcal{P}\Phi_n$ with energy $-E_n$ exists. The corresponding annihilation operator satisfies $\Gamma_{-n} = \Gamma_n^\dagger$. We consider energies below the SC gap and include the excited vortex-bound states (Caroli–de Gennes–Matricon states). The lowest energy state in the system is the Majorana state Φ_M with energy E_M, and its corresponding operator is given by $\Gamma_M = \frac{1}{2}(\gamma_1 - i\gamma_2)$, where γ_1 and γ_2 are two Majorana operators, as shown in Fig. 1. We aim to read out the occupation number $n_M = \Gamma_M^\dagger \Gamma_M$ [or its parity, $(-1)^{n_M} = i\gamma_1\gamma_2$] of this Majorana zero mode.

Expanding the Nambu spinor Ψ in terms of Γ_n,

$$\Psi = \sum_{E_n > 0} (\Phi_n \Gamma_n + \Phi_{-n}\Gamma_n^\dagger), \qquad (2)$$

the MW coupling (1) can be written as

$$\delta H = V_0 \sum_{E_n > 0} q_{n,n}\left(\Gamma_n^\dagger \Gamma_n - \frac{1}{2}\right)$$
$$+ \frac{1}{2}V_0 \sum_{E_n > 0} \sum_{\substack{m \neq n \\ E_m > 0}} [q_{n,m}\Gamma_n^\dagger \Gamma_m + q_{n,-m}\Gamma_n^\dagger \Gamma_m^\dagger + \text{H.c.}]. \quad (3)$$

Here we introduced the matrix elements of the (surface) charge operator $\hat{q} = 2\int d^3\mathbf{r}\rho_e e^{-z/\lambda_{\mathrm{TF}}}$, e.g.,

$$q_{n,m} = -e \int d^3\mathbf{r}(\Phi_n^* \tau_z \Phi_m)e^{-z/\lambda_{\mathrm{TF}}}. \qquad (4)$$

Because the charge operator preserves PHS, the matrix elements obey the same symmetry, encoded by the relations $q_{n,-m} = -q_{-n,m}^*$ and $q_{n,-n} = 0$.

Microwave readout of Majorana parity. In circuit quantum electrodynamics [54], the MW coupling between a resonator and the superconductor allows us to read out the Majorana parity [52]. The electromagnetic fields induced by the resonator interact with the superconductor in the manner described by the Hamiltonian δH, Eq. (3). This interaction influences the complex transmission coefficient $\tau^{(p)}(\omega)$ that relates the output and input photonic fields of the resonator. Under the limit $L_1 C_1 \ll LC$ [see Fig. 1(a)] and frequency close to the cavity resonance $\omega_c = 1/\sqrt{LC_{\mathrm{tot}}}$, we find

$$\tau^{(p)}(\omega) \approx \frac{\kappa}{i(\omega - \omega_c) + \kappa + \frac{i\omega_c \Pi^{(p)}(\omega)}{2C_{\mathrm{tot}}}}, \qquad (5)$$

where $\kappa = 2/(C_{\mathrm{tot}}R^*)$ is the escape rate of the cavity and $p = (-1)^{n_M}$ denotes the Majorana parity. We denote by $\Pi^{(p)}(\omega)$ the parity-dependent charge-charge correlation function. In the time domain, it is given by $\Pi^{(p)}(t) = -\frac{i}{\hbar}\Theta(t)\langle[\hat{q}(t), \hat{q}(0)]\rangle_p$, where $\Theta(t)$ is the Heaviside step function. As shown in Fig. 1(a), $C_{\mathrm{tot}} = C + C_1$, where C and C_1 are the capacitances of the resonator and the superconductor, respectively. The resonator is coupled with capacitance C_κ to the input-output transmission line with resistance R_0, and the effective resistance $R^* = \frac{1+\omega_c^2 C_\kappa^2 R_0^2}{\omega_c^2 C_\kappa^2 R_0}$ incorporates the coupling strength C_κ [55].

The interaction between the resonator and the superconductor induces transitions between the Majorana state and the vortex-bound states localized near the top surface. The correlation function $\Pi^{(p)}$ contains information about these transitions and can be written as a sum (from here we set $\hbar = 1$):

$$\Pi^{(p)}(\omega) = \sum_{l \neq M, E_l > 0} \left(\frac{1}{\omega_l^{(p)} + \omega + i\delta} + \frac{1}{\omega_l^{(p)} - \omega - i\delta}\right)$$
$$[|q_{l,+M}|^2(n_M - n_l) - |q_{l,-M}|^2(n_M - 1 + n_l)], \quad (6)$$

where $\omega_l^{(p)} = E_l + pE_M$ is the transition frequency and E_M, E_l, n_M, and n_l are the energies and occupation numbers of the Majorana state and the bound state l. The infinitesimal level width $\delta > 0$ accounts for causality, and $q_{l,\pm M}$ are the charge matrix elements between the bound state l and occupied or unoccupied ($+$ or $-$M) Majorana state. At low temperatures, in the absence of occupied bound states ($n_l = 0$), we obtain $\Pi^{(+)}(\omega) \propto |q_{l,-M}|^2$ for $n_M = 0$ and $\Pi^{(-)}(\omega) \propto |q_{l,+M}|^2$ for $n_M = 1$. The unequal charge matrix elements $q_{l,+M}$ and $q_{l,-M}$ and transition frequencies $\omega_l^{(p)}$ result in different $\Pi^{(\pm)}(\omega)$, which suggests that the MW coupling can be used to probe the Majorana occupation number n_M.

The critical cavity Q factor. The parity-dependent correlation function $\Pi^{(p)}$ allows for the microwave readout of MZM parity based on the transmission [Eq. (5)]. For simplicity, let

us consider only the first vortex-bound state $l = 1$ on the surface. Our primary interest lies in the strong coupling regime, where the coupling strength $|q_{1,\pm M}|$ greatly exceeds the level width δ. In this regime, the transmission $|\tau^{(p)}|^2$ versus ω displays two parity-dependent peaks at $\omega > 0$. Parity readout is contingent upon the ability to distinguish peaks with different parities, which sets limitations on the cavity Q factor $Q = \frac{\omega_c}{\kappa}$. Here we define a minimum critical cavity Q factor Q_c required for parity discrimination:

$$Q_c^{-1} = \frac{\Delta\Omega_c}{\Omega_c}, \qquad (7)$$

where $\Delta\Omega_c = \Omega_c^{(+)} - \Omega_c^{(-)}$ is the peak separation of two parities in Fig. 1(b), $\Omega_c = \frac{1}{2}(\Omega_c^{(+)} + \Omega_c^{(-)})$ is the average of peak positions, and $\Omega_c^{(\pm)}$ are the shifted resonator frequencies of $p = \pm 1$ parity [56], i.e., $|\tau^{(p)}(\Omega_c^{(p)})|^2 = 1$.

Equation (7) determines the approximate requirement $Q > Q_c$ for the sufficient separation of different parity resonances. There are two variables that affect the critical cavity Q factor Q_c: the parity-dependent charge matrix elements $q_{1,\pm M}$ and the parity-dependent transition energies $\omega_1^{(p)}$ associated with the Majorana energy splitting E_M. We define the dimensionless variable $\zeta_{\pm M} = \sqrt{\frac{U_{\pm M}}{\omega_c}}$ and the capacitive energy $U_{\pm M} = \frac{q_{1,\pm M}^2}{2C_{tot}}$.

In the resonant regime, when the resonator frequency is close to the energy of the first bound state, characterized by $|\omega_c - E_1| \ll \omega_c\zeta$, where $\zeta = \frac{1}{2}(\zeta_{+M} + \zeta_{-M})$, the transmission curve of each parity exhibits two peaks of width κ, separated by $2\omega_c\zeta$. The parity difference causes a shift in the position of the peaks by $\omega_c\delta\zeta - \frac{1}{2}\delta E$, where $\delta\zeta = \zeta_{+M} - \zeta_{-M}$ is the dimensionless transition matrix element difference and δE is the change in resonance frequency given by $\delta E = -2E_M$. It is important to note that these two contributions have opposite effects, which can affect the behavior of the transmission curve in this regime. By setting the shift in peak position equal to the escape rate κ, we obtain

$$Q_c \approx \left| \frac{\omega_c}{\omega_c\delta\zeta + E_M} \right|, \qquad |\omega_c - E_1| \ll \omega_c\zeta. \qquad (8)$$

It is worth mentioning that Q_c diverges at $\delta\zeta = -E_M/\omega_c$ since the peak position does not shift, and, thus, parity detection becomes difficult.

In the detuning regime, where the resonator frequency is significantly detuned from the first bound state's energy ($|E_1 - \omega_c| \gg \omega_c\zeta, E_M$), the full expression for Q_c is more complex compared to the resonant regime (for a detailed derivation, see Ref. [56]). Nevertheless, Q_c can be approximated as

$$Q_c \approx \begin{cases} \left| \frac{E_1^2 - \omega_c^2}{4\omega_c E_1 \zeta\delta\zeta} \right|, & \frac{\delta\zeta}{\zeta} \gg \frac{E_M(E_1^2 + \omega_c^2)}{(E_1^2 - \omega_c^2)E_1}, \\ \frac{(E_1^2 - \omega_c^2)^2}{4\omega_c(E_1^2 + \omega_c^2)E_M\zeta^2}, & \frac{\delta\zeta}{\zeta} \ll \frac{E_M(E_1^2 + \omega_c^2)}{(E_1^2 - \omega_c^2)E_1}, \end{cases} \qquad (9a)(9b)$$

where $|E_1 - \omega_c| \gg \omega_c\zeta, E_M$. The two different forms highlight the parity readout based on the parity dependence of the charge matrix element $\delta\zeta$ or the transition energy E_M. The first form [Eq. (9a)] depends only on the change in the dimensionless charge matrix element difference $\delta\zeta$ as the

parity-dependent factor, while the second form [Eq. (9b)] depends only on the change in transition energy $2E_M$ as the parity-dependent factor.

Model for Fe-based superconductor. In order to estimate the feasibility of the parity readout discussed above, we will use a microscopic Hamiltonian to evaluate the transition matrix element between the Majorana state and the vortex-bound states.

We will analyze a two-band effective Bogoliubov–de Gennes (BdG) model for an Fe-based superconductor [20,57–61]. The Hamiltonian in the Nambu basis $\Psi(\mathbf{k}) = (c_{1\uparrow}, c_{1\downarrow}, c_{2\uparrow}, c_{2\downarrow}, c_{1\uparrow}^\dagger, c_{1\downarrow}^\dagger, c_{2\uparrow}^\dagger, c_{2\downarrow}^\dagger)^T$ can be represented as $H_{SC} = \frac{1}{2} \int dk \Psi^\dagger \mathcal{H}_{SC} \Psi$, where the BdG Hamiltonian $\mathcal{H}_{SC}$ is given by

$$\mathcal{H}_{SC} = \begin{pmatrix} H_0(\mathbf{k}) - \mu & i\Delta_0\sigma_y \\ -i\Delta_0^*\sigma_y & \mu - H_0^*(-\mathbf{k}) \end{pmatrix}, \qquad (10)$$

where $\mu = 5\,\text{meV}$ represents the chemical potential and $\Delta_0 = 1.8\,\text{meV}$ is the bulk pairing gap. In our lattice model, $H_0(\mathbf{k}) = \nu\eta_x(\sigma_x \sin k_x a + \sigma_y \sin k_y a + \sigma_z \sin k_z a) + m(\mathbf{k})\eta_z$, with $m(\mathbf{k}) = m_0 - m_1(\cos k_x a + \cos k_y a) - m_2 \cos k_z a$, where η_i and σ_i represent the Pauli matrices that account for the orbital and spin degrees of freedom, respectively [57]. In this basis, $\mathcal{P} = \tau_x K$, where τ_x represents the Pauli matrix that accounts for the particle-hole degrees of freedom and K denotes complex conjugation. In our numerical simulation, we set $\nu = 10\,\text{meV}$, $a = 5$ nm (the lattice constant), $m_0 = -4\nu, m_1 = -2\nu$, and $m_2 = \nu$, so that the system is in the topological phase [57,60], which can have vortex Majorana zero modes.

In the context of our model, we consider the *s*-wave superconducting pairing potential in the presence of vortices that extend along the z axis. For a single vortex centered at the origin, the pairing term can be expressed as [62]

$$\Delta_{1-v}(w) = \Delta_0 \frac{w}{\sqrt{|w|^2 + \xi^2}}, \qquad (11)$$

where $\xi = 5$ nm represents the characteristic radius of the vortex and $w = x + iy$.

In our specific model [shown in Fig. 1(a)], we consider the presence of two vortices, each hosting a pair of MBSs within the Fe-based superconductor. Assuming the vortices are far apart, we can approximate the pairing term as follows:

$$\Delta_{2-v}(w) = \Delta_0 \frac{w - w_1}{\sqrt{|w - w_1|^2 + \xi^2}} \frac{w - w_2}{\sqrt{|w - w_2|^2 + \xi^2}}, \qquad (12)$$

where w_1 and w_2 correspond to the respective locations of the two vortices (expressed as complex numbers).

The two-vortex pairing term and the BdG Hamiltonian exhibit a Z_2 symmetry represented by $\mathcal{R}_{Z_2} = R(z, \pi)\tau_z\sigma_z$. This operator is characterized by a π rotation around the z axis with respect to the midpoint of the two vortices, taken here as the origin. Its action on a function $f(x, y, z)$ is given by $R(z, \pi)f(x, y, z) = f(-x, -y, z)$. The symmetry operator has eigenvalues ± 1. The manifestation of this symmetry results in the observation of double degeneracy in the system's spectrum, which is evident in the inset of Fig. 2. The operator $\mathcal{R}_{Z_2}$ commutes with the Hamiltonian (1), establishing a selection rule that governs the allowed MW transitions within
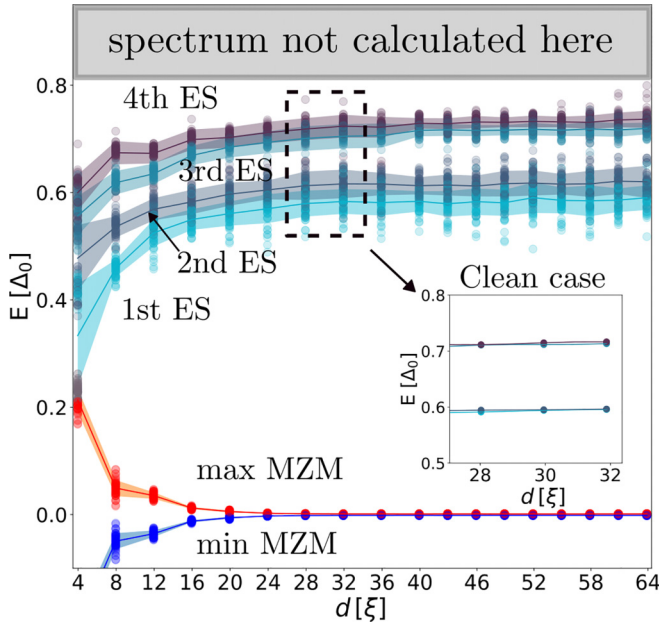
FIG. 2. Eigenvalues vs distances with 50 realizations in the disordered system. The mean values and standard deviations are shown for each energy. The inset shows the spectrum in a clean system, illustrating the degeneracy of excited state pairs at large distances. This degeneracy arises from the symmetry $\mathcal{R}_{Z_2}$ discussed below Eq. (12).
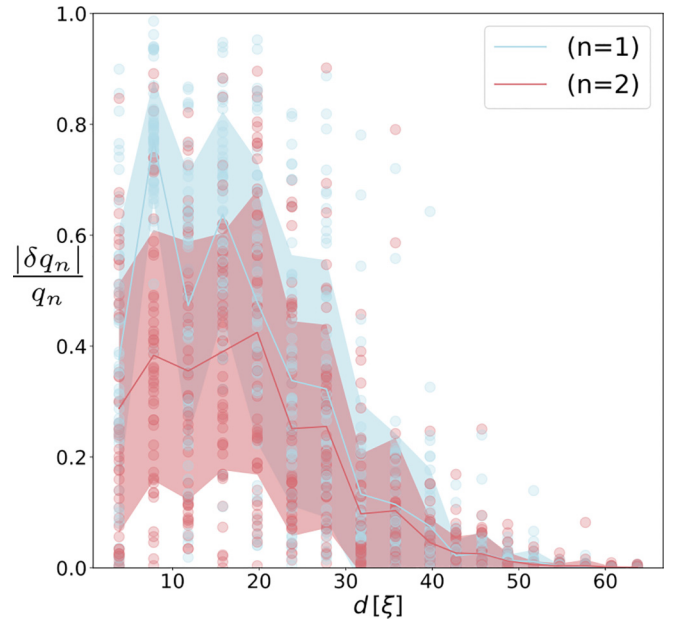

FIG. 3. The ratio of parity-dependent charge difference $|\delta q_n| = |q_{n,+M}| - |q_{n,-M}|$ to the total charge $q_n = |q_{n,+M}| + |q_{n,-M}|$ vs distance for 50 disorder realizations. The charges between MZMs and the two lowest excited states are shown with their mean values and standard deviations. The ratio in the clean system is always 1 due to the selection rule discussed below Eq. (12).

the system. According to the selection rule, transitions within the system can occur only between states that have the same eigenvalues of $\mathcal{R}_{Z_2}$. Since the PHS operator $\mathcal{P} = \tau_x K$ changes the eigenvalue of $\mathcal{R}_{Z_2}$, at least one of the transition matrix elements $q_{n,+M}$, $q_{n,-M}$ vanishes.

However, the presence of random disorder in realistic conditions disrupts the symmetry, resulting in the elimination of the double degeneracy in the spectrum (Fig. 2). Consequently, this compromises the strict adherence to the selection rule. None of the transition matrix elements $q_{n,+M}$ and $q_{n,-M}$ are generally zero (Fig. 3). Thus, in realistic experimental settings, the selection rule is not rigorously maintained.

Numerical studies of two-vortex systems. We employ a numerical approach to investigate a two-vortex system. To perform the numerical analysis, we discretize the Hamiltonian given by Eq. (10) and utilize the KWANT package [63] in PYTHON to implement and solve the corresponding tight-binding model. The system under consideration is a cuboid with dimensions $500 \times 250 \times 25 \, \text{nm}^3$ [refer to Fig. 1(a) for an illustration], discretized with a lattice constant $a = 5$ nm.

We utilize the results obtained in Ref. [56] to calculate the screened electric potential of two vortices [62], which is then included in the real-space version of the Hamiltonian in Eq. (10), similar to the way the chemical potential μ is incorporated. We take the screening length λ_{TF} as one lattice constant. Our investigation encompasses both clean and disordered systems. To model the disorder, we introduce a position-dependent random potential into the Hamiltonian. The disorder potential follows a normal distribution, with standard deviation of this distribution matching the gap Δ_0.

The spectrums and charge matrix elements acquired through numerical computations are depicted in Figs. 2 and 3.

Discussion. We showed that a microwave coupling enables the parity readout of a nonlocal Majorana zero mode hosted in a vortex pair. We quantified the sensitivity of the readout by defining a critical cavity Q factor Q_c [Eqs. (8)–(9b)], required by the resonant cavity coupled to the vortices. To estimate a typical value of Q_c, let us consider a resonant frequency of 5 GHz (much below a typical superconducting gap Δ_0) and effective capacitance of 1×10^{-12} F of a typical coplanar waveguide resonator [55]. In our simulation, we find that the MZM energy E_M for a system with a large vortex separation $d = 36\xi$ can be neglected while the first excited state is approximately at $E_1 \approx 0.58\Delta_0 \gg \omega_c$ (see Fig. 2), implying the system is in the detuning regime. The relevant charge matrix elements are numerically estimated to be $q_1 \approx 0.009e$ and $\delta q_1 \approx 0.002e$, the ratio of which is shown in Fig. 3. In this case, Eq. (9a) gives the required critical cavity Q factor $Q_c \sim 10^8$, which is close to state-of-the-art experimental conditions [64]. Below distance $d \approx 20\xi$, the system is still in the detuning regime of Eq. (9a). There, $Q_c \sim 10^6$, well within the reach of the experiments.

Our method offers a compelling approach to measuring the non-Abelian nature of Majorana zero modes. By employing two resonators to measure quantities $s_z = i\gamma_1\gamma_2$ and $s_x = i\gamma_2\gamma_3$, we can effectively measure two noncommuting parities of MZMs. By monitoring these observables [65,66], we can estimate quasiparticle poisoning time and MZM hybridization E_M. Additionally, incorporating a third resonator to measure $s_y = i\gamma_1\gamma_3$ and an ancillary pair of MZMs would enable measurement-based braiding [34,35,67]

within timescales shorter than the quasiparticle poisoning time when the total parity is conserved (this may be achieved with mesoscopic Coulomb islands [29,67], a likely requirement for universal quantum computation [68]). Alternatively, braiding can be achieved through time-dependent control of MZM hybridization in a nontopologically protected manner [69]. Thus, the resonator-based approach not only allows one to measure the essential quasiparticle poisoning time but also enables one to demonstrate the non-Abelian characteristics of vortex-based MZMs, thus holding significant promise for advancing topological quantum comput-

ing and related technologies. Furthermore, the non-Abelian characteristics prove valuable in discerning between Majoranas and non-Majorana low-energy states induced by pronounced disorder [70].

[1] G. E. Volovik, Fermion zero modes on vortices in chiral superconductors, JETP Lett. **70**, 609 (1999).

[2] N. Read and D. Green, Paired states of fermions in two dimensions with breaking of parity and time-reversal symmetries and the fractional quantum Hall effect, Phys. Rev. B **61**, 10267 (2000).

[3] D. A. Ivanov, Non-Abelian statistics of half-quantum vortices in *p*-wave superconductors, Phys. Rev. Lett. **86**, 268 (2001).

[4] L. Fu and C. L. Kane, Superconducting proximity effect and Majorana fermions at the surface of a topological insulator, Phys. Rev. Lett. **100**, 096407 (2008).

[5] J. D. Sau, R. M. Lutchyn, S. Tewari, and S. Das Sarma, Generic new platform for topological quantum computation using semiconductor heterostructures, Phys. Rev. Lett. **104**, 040502 (2010).

[6] M. Chen, X. Chen, H. Yang, Z. Du, X. Zhu, E. Wang, and H.-H. Wen, Discrete energy levels of Caroli-de Gennes-Matricon states in quantum limit in FeTe$_{0.55}$Se$_{0.45}$, Nat. Commun. **9**, 970 (2018).

[7] D. Wang, L. Kong, P. Fan, H. Chen, S. Zhu, W. Liu, L. Cao, Y. Sun, S. Du, J. Schneeloch, R. Zhong, G. Gu, L. Fu, H. Ding, and H.-J. Gao, Evidence for Majorana bound states in an iron-based superconductor, Science **362**, 333 (2018).

[8] Q. Liu, C. Chen, T. Zhang, R. Peng, Y.-J. Yan, C.-H.-P. Wen, X. Lou, Y.-L. Huang, J.-P. Tian, X.-L. Dong, G.-W. Wang, W.-C. Bao, Q.-H. Wang, Z.-P. Yin, Z.-X. Zhao, and D.-L. Feng, Robust and clean Majorana zero mode in the vortex core of high-temperature superconductor (Li$_{0.84}$Fe$_{0.16}$)OHFeSe, Phys. Rev. X **8**, 041056 (2018).

[9] C. Chen, Q. Liu, T. Z. Zhang, D. Li, P. P. Shen, X. L. Dong, Z.-X. Zhao, T. Zhang, and D. L. Feng, Quantized conductance of Majorana zero mode in the vortex of the topological superconductor (Li$_{0.84}$Fe$_{0.16}$)OHFeSe, Chin. Phys. Lett. **36**, 057403 (2019).

[10] T. Machida, Y. Sun, S. Pyon, S. Takeda, Y. Kohsaka, T. Hanaguri, T. Sasagawa, and T. Tamegai, Zero-energy vortex bound state in the superconducting topological surface state of Fe(Se,Te), Nat. Mater. **18**, 811 (2019).

[11] L. Kong, S. Zhu, M. Papaj, H. Chen, L. Cao, H. Isobe, Y. Xing, W. Liu, D. Wang, P. Fan, Y. Sun, S. Du, J. Schneeloch, R. Zhong, G. Gu, L. Fu, H.-J. Gao, and H. Ding, Half-integer level shift of vortex bound states in an iron-based superconductor, Nat. Phys. **15**, 1181 (2019).

[12] S. Zhu, L. Kong, L. Cao, H. Chen, M. Papaj, S. Du, Y. Xing, W. Liu, D. Wang, C. Shen, F. Yang, J. Schneeloch, R. Zhong,

G. Gu, L. Fu, Y.-Y. Zhang, H. Ding, and H.-J. Gao, Nearly quantized conductance plateau of vortex zero mode in an iron-based superconductor, Science **367**, 189 (2020).

[13] W. Liu, L. Cao, S. Zhu, L. Kong, G. Wang, M. Papaj, P. Zhang, Y.-B. Liu, H. Chen, G. Li, F. Yang, T. Kondo, S. Du, G.-H. Cao, S. Shin, L. Fu, Z. Yin, H.-J. Gao, and H. Ding, A new Majorana platform in an Fe-As bilayer superconductor, Nat. Commun. **11**, 5688 (2020).

[14] L. Kong, L. Cao, S. Zhu, M. Papaj, G. Dai, G. Li, P. Fan, W. Liu, F. Yang, X. Wang, S. Du, C. Jin, L. Fu, H.-J. Gao, and H. Ding, Majorana zero modes in impurity-assisted vortex of LiFeAs superconductor, Nat. Commun. **12**, 4146 (2021).

[15] X. Shi, Z.-Q. Han, P. Richard, X.-X. Wu, X.-L. Peng, T. Qian, S.-C. Wang, J.-P. Hu, Y.-J. Sun, and H. Ding, FeTe$_{1-x}$Se$_x$ monolayer films: towards the realization of high-temperature connate topological superconductivity, Sci. Bull. **62**, 503 (2017).

[16] P. Zhang, K. Yaji, T. Hashimoto, Y. Ota, T. Kondo, K. Okazaki, Z. Wang, J. Wen, G. D. Gu, H. Ding, and S. Shin, Observation of topological superconductivity on the surface of an iron-based superconductor, Science **360**, 182 (2018).

[17] P. Zhang *et al.*, Multiple topological states in iron-based superconductors, Nat. Phys. **15**, 41 (2019).

[18] X.-L. Peng, Y. Li, X.-X. Wu, H.-B. Deng, X. Shi, W.-H. Fan, M. Li, Y.-B. Huang, T. Qian, P. Richard, J.-P. Hu, S.-H. Pan, H.-Q. Mao, Y.-J. Sun, and H. Ding, Observation of topological transition in high-T_c superconducting monolayer FeTe$_{1-x}$Se$_x$ films on SrTiO$_3$(001), Phys. Rev. B **100**, 155134 (2019).

[19] G. Li, S. Zhu, P. Fan, L. Cao, and H.-J. Gao, Exploring Majorana zero modes in iron-based superconductors, Chin. Phys. B **31**, 080301 (2022).

[20] S. Qin, L. Hu, X. Wu, X. Dai, C. Fang, F.-C. Zhang, and J. Hu, Topological vortex phase transitions in iron-based superconductors, Sci. Bull. **64**, 1207 (2019).

[21] T. Machida and T. Hanaguri, Searching for Majorana quasiparticles at vortex cores in iron-based superconductors, Prog. Theor. Exp. Phys. ptad084 (2023).

[22] M. Kheirkhah, Z. Yan, and F. Marsiglio, Vortex-line topology in iron-based superconductors with and without second-order topology, Phys. Rev. B **103**, L140502 (2021).

[23] L.-H. Hu, X. Wu, C.-X. Liu, and R.-X. Zhang, Competing vortex topologies in iron-based superconductors, Phys. Rev. Lett. **129**, 277001 (2022).

[24] A. Banerjee, O. Lesser, M. A. Rahman, H.-R. Wang, M.-R. Li, A. Kringhøj, A. M. Whiticar, A. C. C. Drachmann, C. Thomas, T. Wang, M. J. Manfra, E. Berg, Y. Oreg, A. Stern, and C. M.

Marcus, Signatures of a topological phase transition in a planar Josephson junction, Phys. Rev. B **107**, 245304 (2023).

[25] M. Aghaee *et al.* (Microsoft Quantum), InAs-Al hybrid devices passing the topological gap protocol, Phys. Rev. B **107**, 245423 (2023).

[26] A. Y. Kitaev, Fault-tolerant quantum computation by anyons, Ann. Phys. (NY) **303**, 2 (2003).

[27] C. Nayak, S. H. Simon, A. Stern, M. Freedman, and S. Das Sarma, Non-Abelian anyons and topological quantum computation, Rev. Mod. Phys. **80**, 1083 (2008).

[28] E. Grosfeld, B. Seradjeh, and S. Vishveshwara, Proposed Aharonov-Casher interference measurement of non-Abelian vortices in chiral *p*-wave superconductors, Phys. Rev. B **83**, 104513 (2011).

[29] T. Hyart, B. van Heck, I. C. Fulga, M. Burrello, A. R. Akhmerov, and C. W. J. Beenakker, Flux-controlled quantum computation with Majorana fermions, Phys. Rev. B **88**, 035121 (2013).

[30] S. Tewari, S. Das Sarma, C. Nayak, C. Zhang, and P. Zoller, Quantum computation using vortices and Majorana zero modes of a $p_x + ip_y$ superfluid of fermionic cold atoms, Phys. Rev. Lett. **98**, 010506 (2007).

[31] X. Ma, C. J. O. Reichhardt, and C. Reichhardt, Braiding Majorana fermions and creating quantum logic gates with vortices on a periodic pinning structure, Phys. Rev. B **101**, 024514 (2020).

[32] H.-Y. Ma, D. Guan, S. Wang, Y. Li, C. Liu, H. Zheng, and J.-F. Jia, Braiding Majorana zero mode in an electrically controllable way, J. Phys. D **54**, 424003 (2021).

[33] C. Hua, G. B. Halász, E. Dumitrescu, M. Brahlek, and B. Lawrie, Optical vortex manipulation for topological quantum computation, Phys. Rev. B **104**, 104501 (2021).

[34] P. Bonderson, M. Freedman, and C. Nayak, Measurement-only topological quantum computation, Phys. Rev. Lett. **101**, 010501 (2008).

[35] C.-X. Liu, D. E. Liu, F.-C. Zhang, and C.-K. Chiu, Protocol for reading out Majorana vortex qubits and testing non-Abelian statistics, Phys. Rev. Appl. **12**, 054035 (2019).

[36] B. Sbierski, M. Geier, A.-P. Li, M. Brahlek, R. G. Moore, and J. E. Moore, Identifying Majorana vortex modes via nonlocal transport, Phys. Rev. B **106**, 035413 (2022).

[37] L. Fu and C. L. Kane, Probing neutral Majorana fermion edge modes with charge transport, Phys. Rev. Lett. **102**, 216403 (2009).

[38] A. R. Akhmerov, J. Nilsson, and C. W. J. Beenakker, Electrically detected interferometry of Majorana fermions in a topological insulator, Phys. Rev. Lett. **102**, 216404 (2009).

[39] T. B. Smith, M. C. Cassidy, D. J. Reilly, S. D. Bartlett, and A. L. Grimsmo, Dispersive readout of Majorana qubits, PRX Quantum **1**, 020313 (2020).

[40] D. Razmadze, D. Sabonis, F. K. Malinowski, G. C. Ménard, S. Pauka, H. Nguyen, D. M. T. van Zanten, E. C. T. O'Farrell, J. Suter, P. Krogstrup, F. Kuemmeth, and C. M. Marcus, Radio-frequency methods for Majorana-based quantum devices: Fast charge sensing and phase-diagram mapping, Phys. Rev. Appl. **11**, 064011 (2019).

[41] L. Bretheau, Ç. Ö. Girit, H. Pothier, D. Esteve, and C. Urbina, Exciting Andreev pairs in a superconducting atomic contact, Nature (London) **499**, 312 (2013).

[42] D. J. van Woerkom, A. Proutski, B. van Heck, D. Bouman, J. I. Väyrynen, L. I. Glazman, P. Krogstrup, J. Nygård, L. P. Kouwenhoven, and A. Geresdi, Microwave spectroscopy of spinful Andreev bound states in ballistic semiconductor Josephson junctions, Nat. Phys. **13**, 876 (2017).

[43] L. Tosi, C. Metzger, M. F. Goffman, C. Urbina, H. Pothier, S. Park, A. Levy Yeyati, J. Nygård, and P. Krogstrup, Spin-orbit splitting of Andreev states revealed by microwave spectroscopy, Phys. Rev. X **9**, 011010 (2019).

[44] M. Hays, V. Fatemi, K. Serniak, D. Bouman, S. Diamond, G. de Lange, P. Krogstrup, J. Nygård, A. Geresdi, and M. H. Devoret, Continuous monitoring of a trapped superconducting spin, Nat. Phys. **16**, 1103 (2020).

[45] M. Hays *et al.*, Coherent manipulation of an Andreev spin qubit, Science **373**, 430 (2021).

[46] V. Fatemi, P. D. Kurilovich, M. Hays, D. Bouman, T. Connolly, S. Diamond, N. E. Frattini, V. D. Kurilovich, P. Krogstrup, J. Nygård, A. Geresdi, L. I. Glazman, and M. H. Devoret, Microwave susceptibility observation of interacting many-body Andreev states, Phys. Rev. Lett. **129**, 227701 (2022).

[47] F. J. Matute-Cañadas, C. Metzger, S. Park, L. Tosi, P. Krogstrup, J. Nygård, M. F. Goffman, C. Urbina, H. Pothier, and A. Levy Yeyati, Signatures of interactions in the Andreev spectrum of nanowire Josephson junctions, Phys. Rev. Lett. **128**, 197702 (2022).

[48] J. J. Wesdorp, F. J. Matute-Caňadas, A. Vaartjes, L. Grünhaupt, T. Laeven, S. Roelofs, L. J. Splitthoff, M. Pita-Vidal, A. Bargerbos, D. J. van Woerkom, P. Krogstrup, L. P. Kouwenhoven, C. K. Andersen, A. L. Yeyati, B. van Heck, and G. de Lange, Microwave spectroscopy of interacting Andreev spins, Phys. Rev. B **109**, 045302 (2024).

[49] T. L. Schmidt, A. Nunnenkamp, and C. Bruder, Microwave-controlled coupling of Majorana bound states, New J. Phys. **15**, 025043 (2013).

[50] K. Yavilberg, E. Ginossar, and E. Grosfeld, Fermion parity measurement and control in Majorana circuit quantum electrodynamics, Phys. Rev. B **92**, 075143 (2015).

[51] E. Ginossar and E. Grosfeld, Microwave transitions as a signature of coherent parity mixing effects in the Majorana-transmon qubit, Nat. Commun. **5**, 4772 (2014).

[52] O. Dmytruk, M. Trif, and P. Simon, Cavity quantum electrodynamics with mesoscopic topological superconductors, Phys. Rev. B **92**, 245432 (2015).

[53] J. I. Väyrynen, G. Rastelli, W. Belzig, and L. I. Glazman, Microwave signatures of Majorana states in a topological Josephson junction, Phys. Rev. B **92**, 134508 (2015).

[54] A. Blais, A. L. Grimsmo, S. M. Girvin, and A. Wallraff, Circuit quantum electrodynamics, Rev. Mod. Phys. **93**, 025005 (2021).

[55] M. Göppl, A. Fragner, M. Baur, R. Bianchetti, S. Filipp, J. M. Fink, P. J. Leek, G. Puebla, L. Steffen, and A. Wallraff, Coplanar waveguide resonators for circuit quantum electrodynamics, J. Appl. Phys. **104**, 113904 (2008).

[56] See Supplemental Material at http://link.aps.org/supplemental/10.1103/PhysRevB.109.L180506 for details of cavity Q factor and screened electric potential.

[57] R.-X. Zhang, W. S. Cole, and S. Das Sarma, Helical hinge Majorana modes in iron-based superconductors, Phys. Rev. Lett. **122**, 187001 (2019).

[58] A. Ghazaryan, P. L. S. Lopes, P. Hosur, M. J. Gilbert, and P. Ghaemi, Effect of Zeeman coupling on the Majorana vortex modes in iron-based topological superconductors, Phys. Rev. B **101**, 020504(R) (2020).

[59] C.-K. Chiu, T. Machida, Y. Huang, T. Hanaguri, and F.-C. Zhang, Scalable Majorana vortex modes in iron-based super-conductors, Sci. Adv. **6**, eaay0443 (2020).

[60] Z. Hou and J. Klinovaja, Zero-energy Andreev bound states in iron-based superconductor Fe(Te, Se), arXiv:2109.08200 (2021).

[61] T. Barik and J. D. Sau, Signatures of nontopological patches on the surface of topological insulators, Phys. Rev. B **105**, 035128 (2022).

[62] G. Blatter, M. Feigel'man, V. Geshkenbein, A. Larkin, and A. van Otterlo, Electrostatics of vortices in type-II superconductors, Phys. Rev. Lett. **77**, 566 (1996).

[63] C. W. Groth, M. Wimmer, A. R. Akhmerov, and X. Waintal, Kwant: a software package for quantum transport, New J. Phys. **16**, 063065 (2014).

[64] T. Noguchi, A. Dominjon, M. Kroug, S. Mima, and C. Otani, Characteristics of very high Q Nb superconducting resonators for microwave kinetic inductance detectors, IEEE Trans. Appl. Supercond. **29**, 1 (2019).

[65] U. Vool, I. M. Pop, K. Sliwa, B. Abdo, C. Wang, T. Brecht, Y. Y. Gao, S. Shankar, M. Hatridge, G. Catelani, M. Mirrahimi, L. Frunzio, R. J. Schoelkopf, L. I. Glazman, and M. H. Devoret, Non-Poissonian quantum jumps of a fluxonium qubit due to quasiparticle excitations, Phys. Rev. Lett. **113**, 247001 (2014).

[66] M. Hays, G. de Lange, K. Serniak, D. J. van Woerkom, D. Bouman, P. Krogstrup, J. Nygård, A. Geresdi, and M. H. Devoret, Direct microwave measurement of Andreev-bound-state dynamics in a semiconductor-nanowire Josephson junction, Phys. Rev. Lett. **121**, 047001 (2018).

[67] T. Karzig *et al.*, Scalable designs for quasiparticle-poisoning-protected topological quantum computation with Majorana zero modes, Phys. Rev. B **95**, 235305 (2017).

[68] B. M. Terhal and D. P. DiVincenzo, Classical simulation of noninteracting-fermion quantum circuits, Phys. Rev. A **65**, 032325 (2002).

[69] M. Trif and P. Simon, Braiding of Majorana fermions in a cavity, Phys. Rev. Lett. **122**, 236803 (2019).

[70] B. S. de Mendonça, A. L. R. Manesco, N. Sandler, and L. G. G. V. Dias da Silva, Near zero energy Caroli–de Gennes–Matricon vortex states in the presence of impurities, Phys. Rev. B **107**, 184509 (2023).